International Journal of Adhesion and Adhesives 84 (2018) 27–36

Contents lists available at ScienceDirect

International Journal of Adhesion and Adhesives

journal homepage: www.elsevier.com/locate/ijadhadh

Analysis of the adhesive properties of carbon nanotube- and graphene oxide nanoribbon-dispersed aliphatic epoxy resins based on the Maxwell model

M. Shioya*, Y. Kuroyanagi, M. Ryu, J. Morikawa

Tokyo Institute of Technology, School of Materials and Chemical Technology, Japan

ARTICLE INFO

Keywords:
Epoxy resin
Graphene nanoribbon
Carbon nanotube
Adhesion
Viscoelasticity

ABSTRACT

The viscosity of uncured epoxy resins is usually increased by their incorporation of dispersed fillers such as carbon nanotubes (CNTs). The present authors found that for the aliphatic epoxy resin, i.e. diethylene glycol diglycidyl ether, the viscosity increase is greatly suppressed when graphene oxide nanoribbons (GONRs) are dispersed instead of CNTs. The present study aims to compare the effects of CNT and GONR dispersions in this resin on the adhesive, tensile and thermal properties of the cured resin. GONR dispersions were found to be more effective than CNT dispersions at increasing the fracture toughness, lap shear strength and peel strength of the cured resin. A simple analysis based on a two-element Maxwell model was presented, which reproduced the differences in the temperature and velocity dependences of the lap shear strength and peel strength. This model suggested that the increase in the adhesive strength was due to the increase in the intrinsic adhesive failure energy for the GONR dispersions, while it was due to the increase in the viscoelastic energy dissipation within the resin for the CNT dispersions.

1. Introduction

The demand for lower carbon dioxide emissions and energy consumption has driven the development of stronger and lighter materials such as carbon fibre reinforced composites. The development of high-performance adhesives, as well as stronger reinforcing fibres, is very important in the development of such materials as they can contribute to improvements in matrix properties and offer strong and lightweight jointing techniques between the composites. The most common high-performance adhesives are epoxy resins, which offer good mechanical properties, high temperature tolerance, good chemical and water resistance and good electrical insulation [1].

Epoxy resins, however, are inherently brittle and are often modified by the dispersion of elastomers within them, which improves their toughness [2]. Recently, many attempts have been made to modify epoxy resins [3–10] and other polymers [11–15] by dispersing carbon nanotubes (CNTs) in them; this allows these modified materials to utilize the excellent mechanical, thermal and electrical properties of CNTs; for example, it has been reported that CNT dispersions of 1 mass % increase the fracture toughness of an epoxy resin joint-bonding aluminium plates from 2.0×10^3 to 7.6×10^6 J m^{-2} [4]. It has also been reported that the mechanical properties of CNT-infused materials deteriorate when the CNT content exceeds a certain level due to the formation of aggregates. However, these studies found that the surface modification of CNTs is an effective way to improve their dispersion in polymers [7,8]. Although CNT dispersions are effective in improving the mechanical properties of cured epoxy resins, the inevitable increase in viscosity of uncured resins significantly deteriorates their handling abilities [9].

A few recently developed nanomaterials have received a lot of attention for their potential use as fillers in modified polymers; these are two-dimensional carbon-based nanoparticles such as graphene, graphene nanoribbons (GNRs), graphene oxides (GOs) and graphene oxide nanoribbons (GONRs). GONRs are thin elongated strips of graphene that have high aspect ratios and straight edges decorated with functional groups such as carboxyl groups. They can be produced by the unzipping of CNTs [16], and they can be converted to GNRs by the functional groups at their edges being replaced with groups, such as methyl groups, or hydrogen atoms. The mechanical, rheological and thermal properties of epoxy resins dispersed with several types of carbon-based nanoparticles have been compared in an earlier study [10].

The properties of epoxy resins vary significantly depending on, for instance, their chemical structure, cross-linking density and the curing conditions [17,18]. The most widely used epoxy resin is an aromatic type that is obtained by the condensation of epichlorohydrin with bisphenol, which is in the form of a viscous liquid or a brittle solid, depending on the molecular weight. Cured aromatic epoxy resins have

* Corresponding author.
E-mail address: shioya.m.aa@m.titech.ac.jp (M. Shioya).

https://doi.org/10.1016/j.ijadhadh.2018.01.019
Accepted 11 January 2018
Available online 31 January 2018
0143-7496/ © 2018 The Authors. Published by Elsevier Ltd. This is an open access article under the CC BY license (http://creativecommons.org/licenses/BY/4.0/).

high elastic moduli, high adhesion shear strengths and good chemical resistance. By contrast, aliphatic epoxy resins, such as diethylene glycol diglycidyl ether, yield more flexible cured resins that also have good chemical resistance and good electrical insulation. The uncured resins of this type exhibit lower viscosities than the aromatic epoxy resins; for example, the viscosities of bisphenol A-type and diethylene glycol diglycidyl ether-type commercial epoxy resins are 12–15 and 0.0028 Pa s, respectively, according to manufacturer catalogues. Aliphatic epoxy resins are therefore used as reactive diluents to reduce the viscosity of uncured aromatic epoxy resins. The present authors found that diethylene glycol diglycidyl ether-type epoxy resins dispersed with GONRs display a peculiar behaviour; namely, that the viscosity increase of the uncured resins, which is a significant increase when CNT dispersions are used, can be greatly suppressed by dispersing GONRs instead of CNTs; this allows for the good handling abilities of the resins to be preserved.

In the present study, the effects of CNT and GONR dispersions on the adhesive, tensile and thermal properties of a cured aliphatic epoxy resin were compared. Most previous works on the properties of epoxy resins dispersed with carbon nanoparticles were concerned with aromatic epoxy resins. The present study, however, focused on an aliphatic epoxy resin for the applications where the low viscosity exhibited by uncured resins is of prime importance. A simple model that reproduced the differences in the temperature and velocity dependences of the lap shear strength and peel strength is presented in this study. The effects of the CNT and GONR dispersions were analysed using this model. The lower viscosity of the GONR-dispersed uncured aliphatic epoxy was considered to be related to the shapes and the interactions with the resins, of GONRs; a detailed analysis will be given elsewhere.

2. Materials and methods

2.1. Materials

The epoxy resin used in the present study was diethylene glycol diglycidyl ether (Sakamoto Yakuhin Kogyou Co., LTD., SR-2EG). It was cured using a carboxylic anhydride hardener, i.e. methyl-5-norbornene-2,3-dicarboxylic anhydride (Nippon Kayaku Co., Ltd., Kayahard MCD) and a curing accelerator, i.e. *N*, *N*-dimethylbenzylamine (Aldrich).Their chemical structures are shown in Fig. 1.

Multi-walled carbon nanotubes (MWCNTs, Showa Denko K.K., VGCF-H), with diameters of 150 nm and lengths of 10–20 μm, were used for the fillers and the parent MWCNTs used to produce the GONRs.

GONRs were produced via the unzipping method. 150 mg of MWCNTs were stirred in concentrated H_2SO_4 at room temperature for 1 h, before 750 mg of $KMnO_4$ was added to the mixture; this mixture was stirred at room temperature for 1 h before being stirred for an additional 1 h at 55 °C and reacted at 70 °C for 30 min. After cooling to room temperature, the mixture was poured over 395 g of iced water that had been mixed with 5 mL of H_2O_2, and the resulting mixture was suction filtrated over a polytetrafluoroethylene (PTFE) membrane that had a pore size of 0.45 μm. The remaining product was mixed with 150 mL of water, ultrasonicated for 30 min and mixed with 40 mL of HCl at 5 mol L^{-1} before being stirred and suction filtrated. The remaining product was mixed with 150 mL of ethanol, ultrasonicated for 30 min, mixed with hexane and dried.

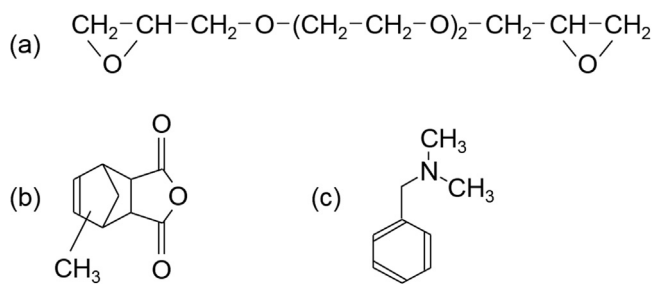

Fig. 1. Chemical structures of (a) the aliphatic epoxy resin, i.e. diethylene glycol diglycidyl ether, (b) the carboxylic anhydride hardener, i.e. methyl-5-norbornene-2,3-dicarboxylic anhydride and the curing accelerator, i.e. *N*, *N*-dimethylbenzylamine.

2.2. Preparation of the filler-dispersed resin

The filler-dispersed epoxy resins were prepared as follows: the fillers were added to an appropriate amount of acetone, ultrasonicated for 2 h and mixed with the epoxy resin; the acetone was then evaporated. The epoxy resin, the hardener and the curing accelerator were mixed to a mass ratio of 10:10:0.55, and they were subjected to ultrasonication for 30 min before being stirred with a planetary centrifugal mixer (Thinkey, ARE-310) at 2,000 rpm for 5 min. The resin was cured at 110 °C for 2 h and then at 150 °C for 1 h. Initially, we compared the effects of the CNT and GONR dispersions at filler contents of 1 mass%. As the GONR dispersion was found to have a greater effect on some of the properties, the CNT content was increased to 2 mass% to see if its effects would be comparable with the 1 mass% GONR dispersion. For the resin that was dispersed with 2 mass% CNT, however, we observed with a scanning electron microscope a slight aggregation of the CNTs.

2.3. Differential scanning calorimetry

The glass transition temperature (T_g) and specific heat at constant pressure (C_p) of the cured resins were determined through differential scanning calorimetry (DSC) by a calorimeter (PerkinElmer Inc., DSC7). 15 mg specimens were heated at a rate of 10 °C min^{-1}, and T_g and C_p were determined using the heating curves of three successive heating–cooling cycles.

2.4. Mechanical tests

The tensile properties of the resins were measured using dumbbell-shaped test pieces of the cured resins, which were 2 mm thick, had gage widths of 4 mm, gage lengths of 29 mm, grip area widths of 12.5 mm and total lengths of 73 mm. All of the mechanical tests were performed using a universal material testing machine (Orientec Co. Ltd., RTC-1350A).

The tensile tests of the cured resins at room temperature were performed at a crosshead rate of 2 mm min^{-1}, with the initial separation between the chucks being 45 mm. Three replicate tests were performed. The tensile modulus and the tensile strength were determined from the stress–strain curves.

The temperature dependence of the tensile modulus for the cured resins was measured using the universal material testing machine and a heating chamber. The initial separation between the chucks was 4.95 mm. The test pieces were cyclically loaded to a stress of 5 MPa and immediately unloaded at a strain rate of 40% min^{-1} at temperature intervals of 1 °C while the temperature was continuously increased at a heating rate of 0.014 °C min^{-1}. The tensile modulus was determined from the stress–strain curves as a function of temperature.

The stress relaxation tests of the cured resins were performed at 40 °C. The separation between the chucks was 4.95 mm. The test pieces were initially kept in the heating chamber at 40 °C for 15 min without stretching before being stretched to a strain of 5% at a strain rate of 60.6% min^{-1}; after this, they were kept at a constant length while the load was measured.

The fracture toughness values of the cured resins at room temperature were measured using three-point bending tests on single-edge notched bend test pieces that had thicknesses (B) of 5 mm, widths (W) of 9 mm and lengths of 73 mm. An initial crack, which had a length (a) of 4 mm, was introduced in the direction of the width of the test pieces through the use of a razor blade. The span (S) between the two lower supporting pins was 36 mm, and the rate at which the upper load pin

was lowered for the bending of the test pieces in the direction of their widths was 1 mm min^{-1}. The test pieces failed in a brittle manner at the maximum load (P). Three or four replicate tests were performed. The mode I fracture toughness (K_{IC}) values of the test pieces were calculated in the plane-strain state as per the ASTM standard D5045-95; this was done using the following equations:

$$K_{IC} = f(a/W)BW^{1/2}P, \tag{1}$$

$$f(x) = 6x^{1/2}\frac{[1.99 - x(1-x)(2.15 - 3.93x + 2.7x^2)]}{(1+2x)(1-x)^{3/2}}. \tag{2}$$

The critical strain energy release rate (G_{IC}) in the plane-strain state can be calculated from K_{IC}, the tensile modulus (E) and the Poisson ratio (ν) using the following equation:

$$G_{IC} = \frac{(1-\nu^2)K_{IC}^2}{E}. \tag{3}$$

Lap shear tests were performed at room temperature with aluminium plates that were 1.5 mm thick, 5 mm wide and 50 mm long; these plates were used as substrates. The aluminium plates were initially polished with abrasive paper, washed with detergent, water and acetone and dried by being blown with hot air. Two aluminium plates were bonded together with the resin and cured as specified in Section 2.2. The adhesive layer was about 0.2 mm thick and the overlap was 3 mm long. Both ends of the bonded aluminium plates were loaded at a rate of 1 mm min^{-1}.

The T-peel tests were performed using aluminium sheets that were 0.1 mm thick, 25 mm wide and 150 mm long; the sheets acted as substrates. The aluminium sheets were treated in a similar manner to that performed on the aluminium plates in the lap shear tests; two aluminium sheets were then bonded together with the resin and cured as specified in Section 2.2. The thickness of the adhesive layer was controlled by a PTFE tape that was 0.2 mm thick, which was sandwiched between the two aluminium plates that were bonded by the resin. The applicability of the temperature–time superposition principle was investigated using T-peel tests that were performed at temperatures above T_g and at various peeling rates.

3. Results

The changes in the specific heat (C_p) of the cured neat resin as functions of temperature are shown in Fig. 2, where the heating curves of three successive heating–cooling cycles of DSC measurements are shown. The endothermic peak at approximately 56 °C is due to the enthalpy relaxation, which was observed for all of the neat and filler-dispersed resins only for the first heating. The rapid increase in C_p at around 49 °C was due to commencement of micro-Brownian motion at the glass transition temperature. The glass transition temperature (T_g) and the difference in the specific heat caused by the glass transition (ΔC_p) were determined as shown in Fig. 2.

In Fig. 3, T_g, C_p at both 30 °C and 90 °C and ΔC_p are plotted against the filler content for the neat and filler-dispersed cured resins. The filler dispersion was found to barely influence T_g. In the glassy state below T_g, C_p decreased at a similar rate to the increases in the CNT and GONR content. In the rubbery state above T_g, C_p did not change with increases in the CNT dispersion but it decreased as the GONR dispersion increased.

The tensile moduli, tensile strengths and fracture toughness values of the neat and filler-dispersed cured resins at room temperature are compared in Fig. 4. The tensile moduli and strengths were shown to hardly change as the filler dispersions increased. A GONR dispersion of the same content as a CNT dispersion was found to be more effective in increasing the fracture toughness. The stress relaxation curves at 40 °C and the relative change in the tensile moduli as a function of temperature for the neat and filler-dispersed cured resins are shown in Fig. 5(a) and (b), respectively. Both of the CNT and GONR dispersions

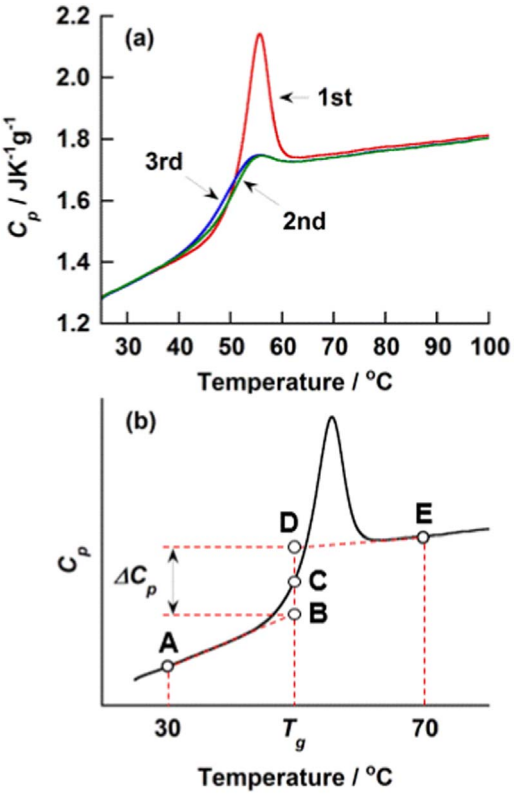

Fig. 2. (a) Specific heat (C_p) as a function of temperature for aliphatic epoxy resins during the heating processes of three successive heating–cooling cycles, and (b) a schematic of the method for determining the glass transition temperature (T_g) and the difference in the specific heat caused by the glass transition (ΔC_p). Lines AB and DE are tangent to the DSC curve at 30 °C and 70 °C, respectively, and segments BC and CD have equal lengths.

were found to be effective in both suppressing the stress relaxation at temperatures around T_g and reducing the tensile modulus above T_g.

For both the lap shear and T-peel tests of the neat and filler-dispersed resins, the test pieces failed at the interfaces between the adhesive and the substrate. The lap shear strength at a constant shear rate of 1 mm min^{-1} and the T-peel strength at various peeling rates are shown as functions of temperature in Figs. 6(a) and 7, respectively. As the temperature increased, the lap shear strength markedly decreased, while the peel strength achieved a maximum value at a temperature around T_g. Similar behaviours have been reported for aromatic epoxy resins [17].

4. Discussion

The peel strengths of simple viscoelastic solids have been found to follow the temperature–time superposition principle at various temperatures and peeling rates [19]; more specifically, the peel strength at an arbitrary temperature (T) and an arbitrary peeling rate ($v_M(T)$) equals the peel strength at T_g and a reduced peeling rate ($v_M^*(T_g)$); these can be determined by the following Williams, Landel and Ferry equation:

$$v_M^*(T_g) = a_T v_M(T), \tag{4}$$

$$\log(a_T) = \log\left(\frac{\tau(T)}{\tau(T_g)}\right) = \frac{-17.4(T - T_g)}{51.6K + T - T_g}, \tag{5}$$

where the shift factor (a_T) is related to the relaxation times at an arbitrary temperature ($\tau(T)$) and at a reference temperature ($\tau(T_g)$), which was chosen to be T_g in this study. Therefore, lowering the temperature at a constant peeling rate works in the same direction as increasing the peeling rate at a constant temperature. By using Eqs. (4) and (5), we

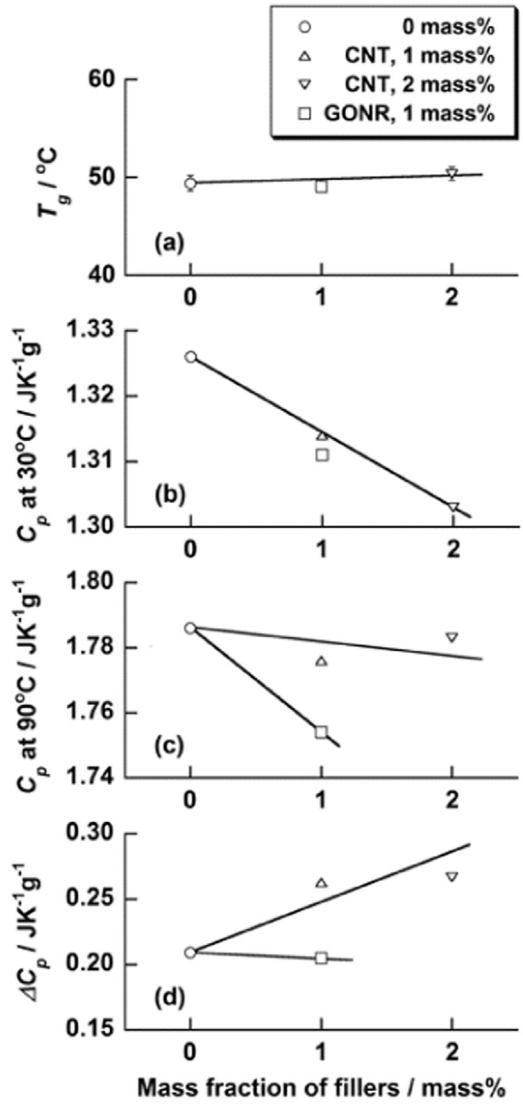

Fig. 3. (a) Glass transition temperature (T_g), specific heat (C_p) at (b) 30 °C and (c) 90 °C and (d) difference in the specific heat caused by the glass transition (ΔC_p) of neat and filler-dispersed aliphatic epoxy resins as a function of filler content. The maximum values of the standard deviations of T_g and C_p are 0.8 °C and 0.007 J K^{-1} g^{-1}.

were able to convert the shear and peeling rates at various temperatures in Figs. 6(a) and 7 into the reduced shear and peeling rates, respectively, at T_g for individual materials. The lap shear strength and peel strength are plotted against these reduced rates in Figs. 6(b) and 8, respectively. Fig. 8 confirms that the peeling strength changes with the reduced peeling rate along the master curves of individual materials.

Fig. 6 indicates that, in comparison to the CNT dispersions at 1 and 2 mass%, the GONR dispersion at 1 mass% was more effective in increasing the lap shear strength below T_g at a shear rate of 1 mm min^{-1}, and at T_g and shear rates larger than 1 mm min^{-1}. Fig. 8(e) indicates that the peel strength was barely influenced by the CNT dispersion at 1 mass%, while it was increased by the GONR dispersion at 1 mass% in the region of the reduced peeling rate below 10^4 mm min^{-1} at T_g. At a low reduced peeling rate of 0.01 mm min^{-1}, the GONR dispersion at 1 mass% was found to be comparable to the CNT dispersion at 2 mass%.

The following can be considered to be the reasons for the differences in the temperature and rate dependences of the lap shear strength and the peel strength: the peel strength (P_d) is defined as being the load divided by the thickness of the test piece (B), and it is measured while the test piece is continuously peeled. In this case, P_d indicates the work required to peel a unit area (as the work required to peel an area $B\Delta L$ is given by $(P_dB)\Delta L$). For the lap shear test, however, the overlap does not slip off until failure, and the lap shear strength (T_d) is the maximum static stress applied up until failure; this parameter is not related to the work done. This difference between how the lap shear strength and peel strength are calculated results in them having different temperature and rate dependences.

This interpretation can be verified by a simple analysis involving a generalized Maxwell model: as shown in Fig. 9, the adhesive layer is modelled by a number of Maxwell models that are aligned to be parallel to the interface for the lap shear test, but the models are aligned perpendicularly to the interface for the peeling test. In general, when a brittle solid that already has a crack is subjected to an increasing tensile load, the crack starts to propagate at the moment when both the energy criterion and stress criterion are satisfied [20]. The energy criterion is that the energy required to create a new crack surface is supplied due to the release of the elastic strain energy that accompanies the crack propagation. The stress criterion is that the stress required to separate atoms or molecules is applied at the crack tip. In the peel test, a large concentration of stress occurs at the peel front; this allows the stress criterion to be satisfied earlier, and peeling starts to propagate at the moment when the energy criterion is satisfied. In the lap shear tests, the shear stress is not uniformly distributed along the overlap; rather, it is concentrated at the ends of the overlap because of the tensile deformation of the substrates (this is called the shear lag effect) [21]. It can be considered, therefore, that a shear fracture in the lap shear tests is governed by the energy criterion for a relatively tough adhesive. When a shear failure begins at the edges of the initial overlap, it propagates through the entire overlap because the shear stress at the edges of the remaining overlap increases as the length of the remaining overlap decreases. The failure, or debonding, of the test pieces in our study was judged to occur if the energy required to create a new crack surface (W_d) was stored in the Maxwell model at the edges of the overlap for the lap shear tests, and at the peel front for the peel tests; the time it takes (t_d) for the Maxwell model located at these positions to go from starting to be stretched until failure is determined by this condition. The lap shear strength (T_d) is proportional to the stress of the Maxwell model at the edges of the overlap at t_d, while the peel strength (P_d) is proportional to the total work done to the Maxwell model at the peel front over t_d. In the case where the Maxwell model is stretched at a constant strain rate (ν_M), the following relations can be derived, as demonstrated in the Appendix A:

$$\log \nu_M - \frac{1}{2}\log(c_D W_d) = -\log(t_d) - \frac{1}{2}\log\left(\sum\nolimits_p G_p(t_d/\tau_p)^{-2}[1-\exp(-t_d/\tau_p)]^2\right), \tag{6}$$

$$\frac{c_T T_d}{\sqrt{W_d}} = \frac{\sum_p G_p(t_d/\tau_p)^{-1}[1-\exp(-t_d/\tau_p)]}{\sqrt{\sum_p G_p(t_d/\tau_p)^{-2}[1-\exp(-t_d/\tau_p)]^2}}, \tag{7}$$

$$\frac{c_P P_d}{W_d} = \frac{\sum_p G_p(t_d/\tau_p)^{-2}[\exp(-t_d/\tau_p)+(t_d/\tau_p)-1]}{\sum_p G_p(t_d/\tau_p)^{-2}[1-\exp(-t_d/\tau_p)]^2}, \tag{8}$$

where the summation is taken over all of the elements in a generalized Maxwell model specified by the index (p). The shear stress distribution along the overlap during the lap shear tests can be incorporated into Eq. (7) by considering c_T as being proportional to the ratio of the average stress against the maximum stress in the overlap. Eqs. (7) and (8) show that T_d and P_d, respectively, take the same values at different temperatures if t_d/τ_p is kept constant for different values of τ_p, which are calculated from the temperatures by using Eq. (5). On the other hand, Eq. (6) shows that t_d/τ_p can be kept constant by changing ν_M so that ν_M t_d is kept constant, which results in Eq. (4). This explains the applicability of the temperature–time superposition principle to both T_d and P_d.

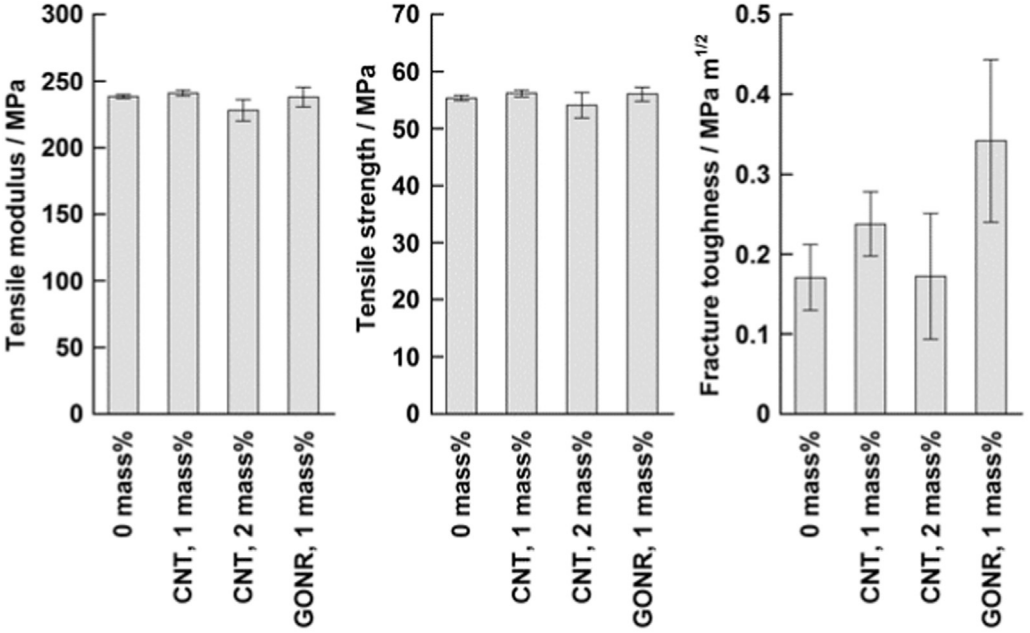

Fig. 4. Tensile modulus, tensile strength and fracture toughness of neat and filler-dispersed aliphatic epoxy resins at room temperature. The error bars indicate the standard deviation.

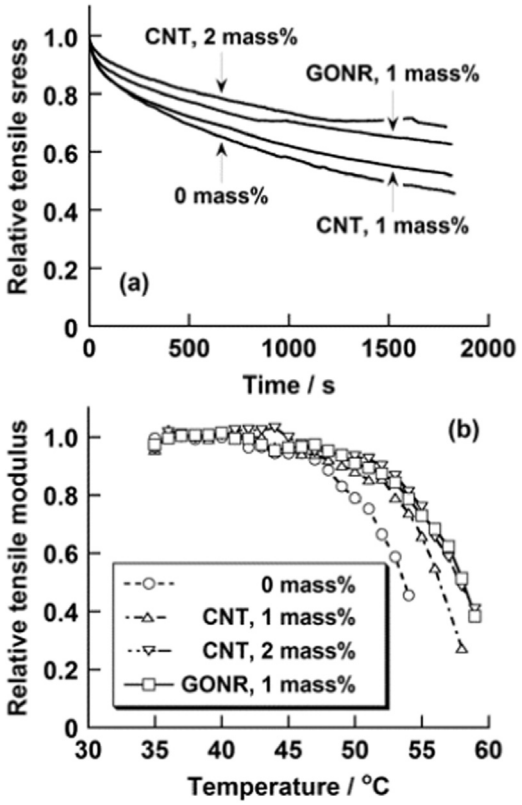

Fig. 5. (a) Relative changes in the tensile stress as a function of time at 40 °C due to stress relaxation, and (b) relative changes in the tensile modulus as a function of temperature for neat and filler-dispersed aliphatic epoxy resins.

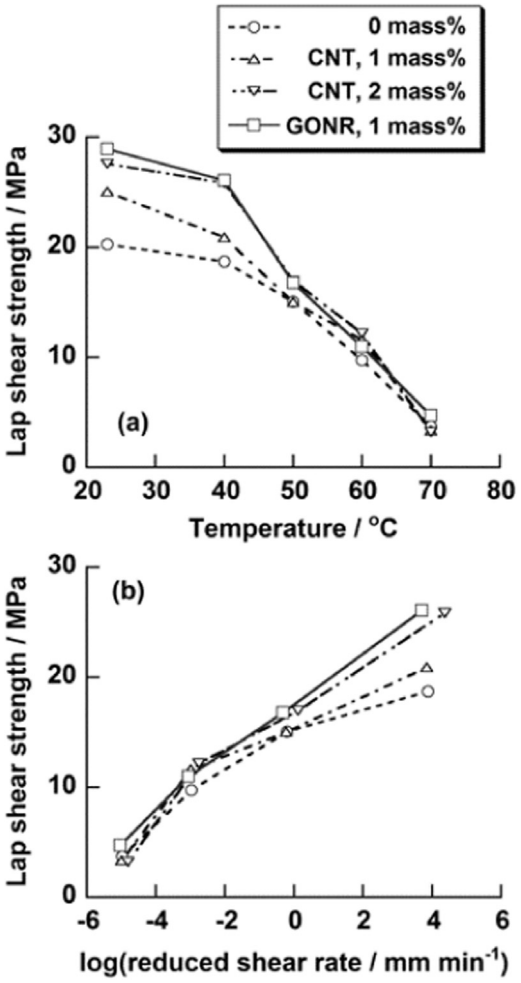

Fig. 6. Changes in the lap shear strength (a) as a function of temperature at a shear rate of 1 mm min^{-1} and (b) as a function of the reduced shear rate at glass transition temperatures for the neat and filler-dispersed aliphatic epoxy resins.

For amorphous thermoplastics, the viscoelasticity above T_g can be most simply represented by a Maxwell model consisting of two elements with a shorter relaxation time (τ_1) and a longer relaxation time (τ_2), which represent the micro- and macro-Brownian motions of the molecular chains, respectively. For thermosetting resins like epoxy resins, the macro-Brownian motion is prevented by crosslinks, which is characterized by an infinitely long relaxation time for τ_2. A calculation

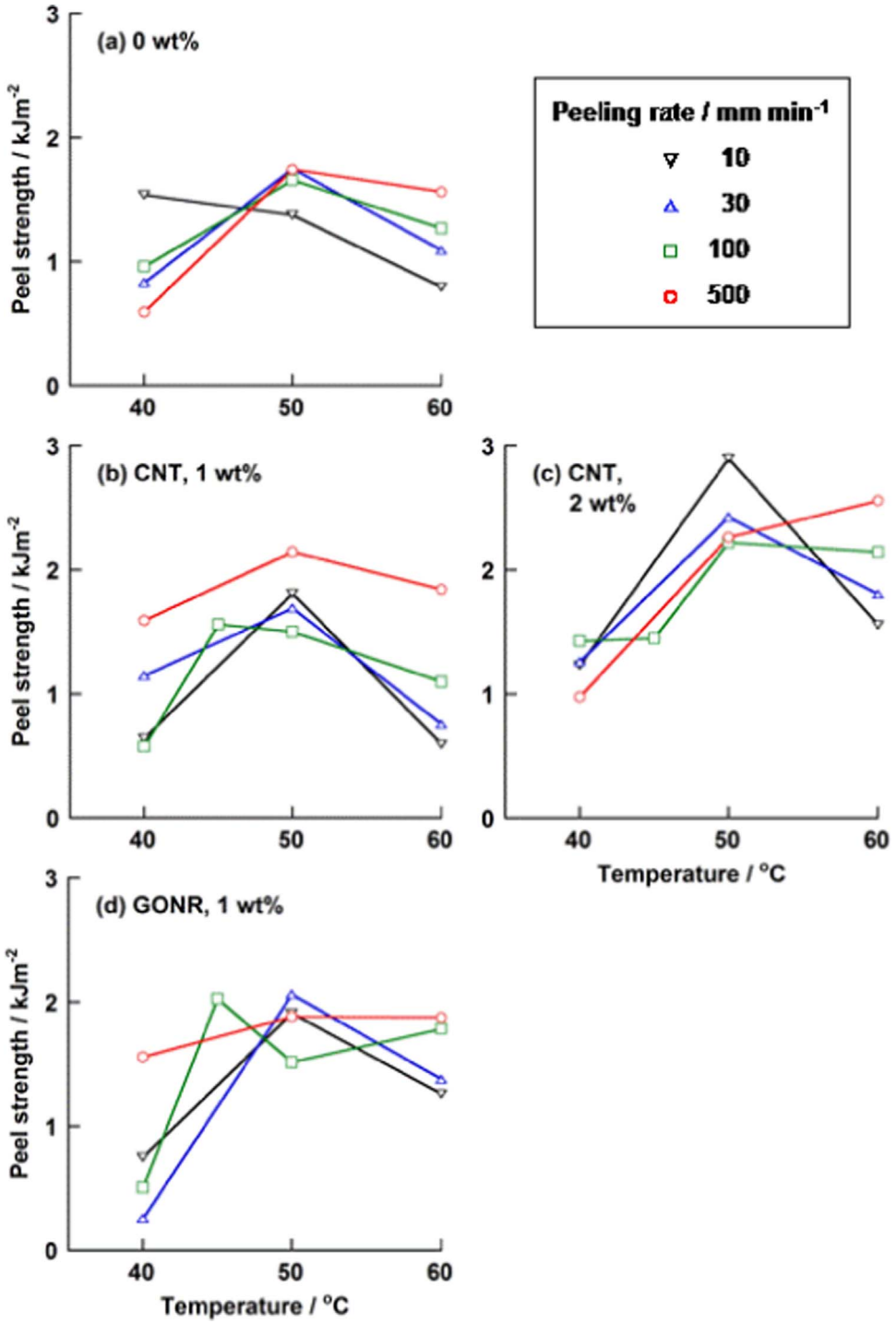

Fig. 7. Changes in the T-peel strength as a function of temperature at various peeling rates for both neat and filler-dispersed aliphatic epoxy resins.

was made using a two-element Maxwell model, where $\tau_1 = 1$ in the same unit as t_d, τ_2 is infinitely long and $G_2/G_1 = 0.01$, which means that the second element consists solely of a spring that has a much smaller elastic modulus than the spring of the first element. The values of log v_M, T_d and P_d were calculated using Eqs. (6)–(8) with the help of Eqs. (A13)–(A15) as functions of t_d. T_d and P_d were then obtained as functions of log v_M by associating the values of log v_M, T_d and P_d with the same value of t_d. The results of the calculation shown in Fig. 10 qualitatively reproduce the different temperature and rate dependences of the lap shear strength and peel strength.

Anderson and Kinloch have shown for a rubber-rigid substrate joint that the adhesive failure energy is the sum of the intrinsic adhesive failure energy required to propagate a crack in the absence of a viscoelastic energy loss and the viscoelastic energy dissipation within the rubber, and they showed that the latter is proportional to the former [19]. This led to the adhesive failure energy being expressed in the form of the product of the intrinsic adhesive failure energy and a multiplying factor that is temperature- and peeling rate-dependent. Eq. (7) is in accordance with their formulation where P_d is given by the product of W_d and a multiplying factor given by the right-hand side of this equation. In addition, Eq. (8) shows that T_d is represented by a product of $W_d^{1/2}$ and a multiplying factor given by the right-hand side of the equation, which is in a different form to that of P_d.

By examining the experimental results based on Eq. (7), it seems as

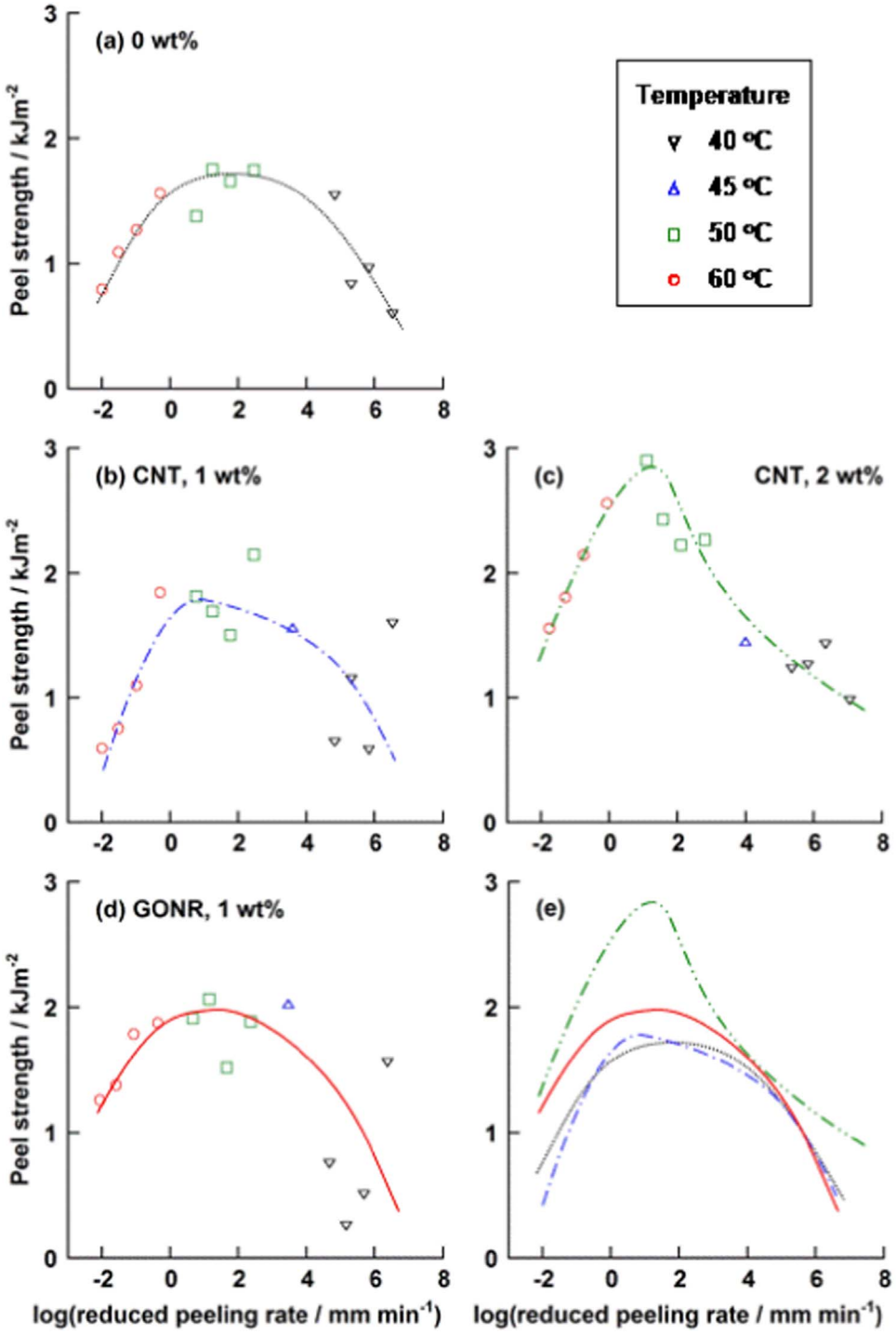

Fig. 8. Master curves of the T-peel strength as a function of the reduced peeling rate at glass transition temperatures for (a) neat, (b)–(d) filler-dispersed aliphatic epoxy resins and (e) all of the resins.

though the mechanisms of the CNT and GONR dispersions increase the adhesive strength differently. The increases in P_d and T_d due to the GONR dispersion are due to the increase in W_d, which we were able to identify from the marked increase in the fracture toughness in Fig. 4. The critical strain energy release rate (G_{IC}) of the GONR-dispersed resin was calculated using Eq. (3), and it was found to be 0.4 kJ m^{-2} when the value of the Poisson ratio was assumed to be 0.4. If this value is used for W_d, the multiplying factor is calculated to be about 5 at the maximum peel strength of 2.0 kJ m^{-2}. The multiplying factor is, however, considered to be much larger than this value because the viscoelastic contribution is included in G_{IC} and W_d is much smaller than G_{IC}. In the case of the CNT dispersion, however, the increases in P_d and T_d are due to the increase in the multiplying factor, as suggested by the smaller increase in the fracture toughness.

The static mechanical properties of resins dispersed with stiffer and stronger fillers can be modelled most simply by parallel and series models if uniform strain and uniform stress over two components, respectively, are assumed. The tensile modulus of the parallel model increases in proportion to the filler content; however, the tensile modulus of the series model is governed by the modulus of the less stiff phase at a low filler content, and a very high filler content is needed for the tensile modulus to be increased. Fig. 4 shows that the tensile modulus of

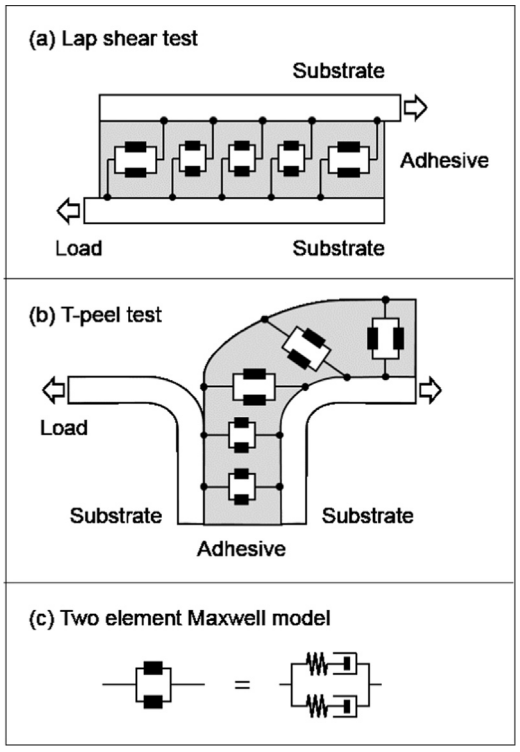

Fig. 9. Modelling of (a) the lap shear test and (b) the T-peel test using (c) a two-element Maxwell model.

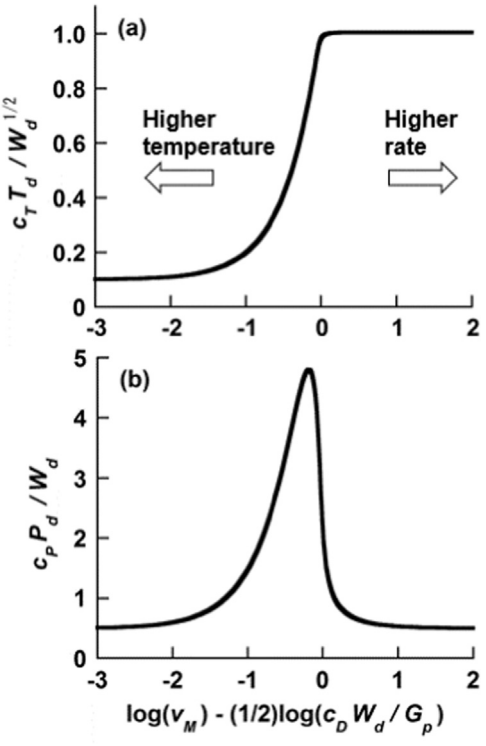

Fig. 10. (a) Lap shear strength and (b) peel strength of the model shown in Fig. 9 as a function of the peeling rate and shear rate (v_M), respectively. The same unit was used for v_M and τ_1^{-1}.

the resin at room temperature is almost uninfluenced by the fillers, which suggests that the tensile properties of the filler-dispersed resins used in the present study can be represented by a series model. At temperatures near or above T_g, the effects of the fillers in both suppressing the stress relaxation and reducing the tensile modulus as a function of temperature are revealed; this was likely due to the larger difference in the tensile moduli between the fillers and the resins at these temperatures as compared with the temperatures below T_g.

Tensile failures in series models are a result of failures in the weaker phase without any contribution from the stronger phase; this is in accordance with the results shown in Fig. 4, which indicate that the tensile strength was not influenced by the fillers. Although the tensile strength was mostly uninfluenced, the fracture toughness and adhesive strength were increased by the fillers, which is because failure in the tensile tests is governed by the stress criterion, while failure in the tests used to measure the fracture toughness and adhesive strength is governed by the energy criterion.

With respect to the restriction of local molecular motion by the fillers, it was manifested as the decrease in the specific heat below T_g. Above T_g, this effect was prominent only for GONRs; this was probably due to their stronger interaction with the resins, which was likely due to both the functional groups at the edges and their having a larger specific surface area than the CNTs.

5. Conclusions

We investigated and compared the effects of CNT and GONR dispersions on the adhesive, tensile and thermal properties of a cured aliphatic epoxy resin, i.e. diethylene glycol diglycidyl ether. These fillers were found to increase the lap shear strength and peel strength, and they suppressed the stress relaxation near T_g and the reduction in the tensile modulus above T_g, as well as decrease the specific heat below T_g. However, these fillers were found to have little influence on the tensile modulus and strength at room temperature and at T_g. A GONR dispersion of the same content as a CNT dispersion was found to be more effective in increasing the fracture toughness, lap shear strength and peel strength of the cured resin, and was also more effective in decreasing the specific heat at temperatures above T_g. The peel strengths of the neat and filler-dispersed resins were measured at various temperatures and peeling rates and found to follow the temperature–time superposition principle.

A simple analysis using a two-element Maxwell model reproduced the differences in the temperature and rate dependences between the lap shear strength and peel strength. This model suggests that the increase in the adhesive strength was due to an increase in the intrinsic adhesive failure energy for GONR dispersions, while for the CNT dispersions, it was due to the increase in the viscoelastic energy dissipation within the resin. The advantages of the GONR dispersions over the CNT dispersions used in this study were that the viscosity increase of the uncured resin was markedly suppressed, while the adhesive strength and thermomechanical properties of the resin were increased.

Appendix A. Analysis of adhesive strength based on the Maxwell model

The viscoelasticity of an adhesive is represented by a generalized Maxwell model that consists of several elements assembled in parallel. The following parameters are defined for the generalized Maxwell model:

G_p = elastic modulus of a spring in the p-th element of the Maxwell model

η_p = viscosity of a dashpot in the p-th element of the Maxwell model

$\tau_p = \eta_p/G_p$ = relaxation time of the p-th element of the Maxwell model

$\sigma_M(t)$, γ_M = stress and strain of the Maxwell model at a time, t, after

stretching has started
σ_p = stress of the p-th element of the Maxwell model
$\gamma_{p,s}$ = strain of a spring in the p-th element of the Maxwell model
ν_M = strain rate of the Maxwell model and all of its elements
$W_M(t)$ = work done to the Maxwell model up to time t
$W_s(t)$ = elastic energy stored in all of the springs in the Maxwell model up to time t
W_d = energy required to create a new crack surface of a unit area
t_d = time that has elapsed from when stretching started until failure occurs
k_D, k_T, k_P, c_D, c_T, c_P = constants independent of ν_M.

When the generalized Maxwell model is stretched at a constant strain rate, $\sigma_M(t)$, $W_M(t)$ and $W_s(t)$ change with time as follows:

$$\sigma_M(t) = \nu_M \sum_p G_p\tau_p[1 - \exp(-t/\tau_p)], \tag{A1}$$

$$W_s(t) = \sum_p \int \sigma_p d\gamma_{p,s} = \frac{1}{2}{\nu_M}^2 \sum_p G_p{\tau_p}^2[1 - \exp(-t/\tau_p)]^2, \tag{A2}$$

$$W_M(t) = \sum_p \int \sigma_p d\gamma_M = {\nu_M}^2 \sum_p G_p{\tau_p}^2[\exp(-t/\tau_p) + (t/\tau_p) - 1], \tag{A3}$$

where the integrations are carried out from $t = 0$ to t_d. If shear failure and peeling are governed by the energy criterion, t_d is determined by W_d through the following equation:

$$W_d = k_D W_s(t_d). \tag{A4}$$

The lap shear strength (T_d) is proportional to the stress of the Maxwell model at t_d:

$$T_d = k_T \sigma_M(t_d). \tag{A5}$$

The peel strength (P_d) is proportional to the total work done to the Maxwell model until t_d:

$$P_d = k_P W_M(t_d). \tag{A6}$$

By combining these equations, the following equations can be obtained:

$$\log \nu_M - \frac{1}{2}\log(2W_d/k_D) = -\log(t_d) - \frac{1}{2}\log\left(\sum_p G_p(t_d/\tau_p)^{-2}[1 - \exp(-t_d/\tau_p)]^2\right), \tag{A7}$$

$$\sqrt{\frac{k_D}{2W_d}}\frac{T_d}{k_T} = \frac{\sum_p G_p(t_d/\tau_p)^{-1}[1 - \exp(-t_d/\tau_p)]}{\sqrt{\sum_p G_p(t_d/\tau_p)^{-2}[1 - \exp(-t_d/\tau_p)]^2}}, \tag{A8}$$

$$\frac{k_D P_d}{2k_P W_d} = \frac{\sum_p G_p(t_d/\tau_p)^{-2}[\exp(-t_d/\tau_p) + (t_d/\tau_p) - 1]}{\sum_p G_p(t_d/\tau_p)^{-2}[1 - \exp(-t_d/\tau_p)]^2}. \tag{A9}$$

Eqs. (6)–(8) can be obtained by using the following coefficients:

$$c_D = 2/k_D, \tag{A10}$$

$$c_T = \sqrt{k_D}/(\sqrt{2}k_T), \tag{A11}$$

$$c_P = k_D/(2k_P). \tag{A12}$$

If the q-th element of the Maxwell model consists solely of a spring, this element makes the following contributions to the summations in the right-hand side of Eqs. (A1)–(A3):

$$G_q\tau_q[1 - \exp(-t_d/\tau_q)] = G_q t_d, \tag{A13}$$

$$G_q{\tau_q}^2[\exp(-t_d/\tau_q) + (t_d/\tau_q) - 1] = \frac{1}{2}G_q{t_d}^2, \tag{A14}$$

$$G_q{\tau_q}^2[1 - \exp(-t_d/\tau_q)]^2 = G_q{t_d}^2. \tag{A15}$$

References

[1] Astrom BT. Manufacturing of polymer composites. London: Chapman & Hall; 2002.
[2] Bagheri R, Marouf BT, Pearson RA. Rubber-toughened epoxies: a critical review. J Macromol Sci Polym Rev 2009;49:201–25.
[3] Gerson AL, Bruck HA, Hopkins AR, Segal KN. Curing effects of single-wall carbon nanotube reinforcement on mechanical properties of filled epoxy adhesives. Compos Part A-Appl Sci 2010;41:729–36.
[4] Yu S, Tong MN, Critchlow G. Use of carbon nanotubes reinforced epoxy as adhesives to join aluminum plates. Mater Des 2010;31:S126–9.
[5] Srivastava VK. Effect of carbon nanotubes on the strength of adhesive lap joints of C/C and C/C–SiC ceramic fibre composites. Int J Adhes Adhes 2011;31:486–9.
[6] Han Z, Fina A. Thermal conductivity of carbon nanotubes and their polymer nanocomposites: a review. Prog Polym Sci 2011;36:914–44.
[7] Wolf A, Buchman A, Eitan A, Fine T, Nevo Y, Heyman A, et al. Improved adhesives containing CNT/SP1 nano fillers. J Adhes 2012;88:435–51.
[8] Zhang J, Luo R, Yang C. A multi-wall carbon nanotube-reinforced high temperature resistant adhesive for bonding carbon/carbon composites. Carbon 2012;50:4922–5.
[9] Sydlik SA, Lee J-H, Walish JJ, Thomas EL, Swager TM. Epoxy functionalized multi-walled carbon nanotubes for improved adhesives. Carbon 2013;59:109–20.
[10] Jojibabu P, Jagannatham M, Haridoss P, Ram GDJ, Deshpande AP, Bakshi SR. Effect of different carbon nano-fillers on rheological properties and lap shear strength of epoxy adhesive joints. Compos Part A-Appl Sci 2016;82:53–64.

[11] Kobayashi H, Shioya M, Tanaka T, Irisawa T. Synchrotron radiation small-angle X-ray scattering study on fracture process of carbon nanotube/poly(ethylene terephthalate) composite films. Compos Sci Technol 2007;67:3209–18.
[12] Kobayashi H, Shioya M, Tanaka T, Irisawa T, Sakurai S, Yamamoto K. A comparative study of fracture behavior between carbon black/poly(ethylene terephthalate) and multiwalled carbon nanotube/poly(ethylene terephthalate) composite films. J Appl Polym Sci 2007;106:152–60.
[13] Fujihira K, Irisawa T, Kobayashi H, Shioya M. Specimen geometry dependent effects of vapor grown carbon fibers on fracture toughness of polyamide 6. Int J Polym Technol 2009;1:35–41.
[14] Irisawa T, Kobayashi H, Fujihira K, Shioya M, Kaneko J. A method to determine wear rates of fibers and its application to polymeric fibers added with inorganic fillers. Wear 2010;268:1148–56.
[15] Irisawa T, Takamura T, Momozono S, Kaneko J, Shioya M. Analysis on abrasive wear rate of VGCF/polyamide 6 composite fibers. Tribol Online 2011;6:207–18.
[16] Kosynkin DV, Higginbotham AL, Sinitskii A, Lomeda JR, Dimiev A, Price BK, et al. Longitudinal unzipping of carbon nanotubes to form graphene nanoribbons. Nature 2009;458:872–6.
[17] Shimbo M, Iwakoshi M, Ochi M. Properties of cured epoxy resins. J Adhes Soc Jpn 1974;10:161–8.
[18] Schneider NS, Gillham JK. TBA studies of prepreg curing behavior. Polym Compos 1980;1:97–102.
[19] Andrews EH, Kinloch AJ. Mechanics of adhesive failure I. Proc R Soc Lond A 1973;332:385–99.
[20] Shioya M, Inoue H, Sugimoto Y. Reduction in tensile strength of polyacrylonitrile-based carbon fibers in liquids and its application to defect analysis. Carbon 2013;65:63–70.
[21] Lubowiecka I, Rodrı´guez M, Rodrı´guez E, Martı´nez D. Experimentation, material modelling and simulation of bonded joints with a flexible adhesive. Int J Adhes Adhes 2012;37:56–64.